Analysis of End Effects in Diagonal Type MHD Generator by Means of Equivalent Circuit

AUTHOR(S):

YOSHIDA, Masaharu; UMOTO, Jūrō

CITATION:

YOSHIDA, Masaharu ...[et al]. Analysis of End Effects in Diagonal Type MHD Generator by Means of Equivalent Circuit. Memoirs of the Faculty of Engineering, Kyoto University 1978, 39(4): 504-522

ISSUE DATE:

1978-01-31

URL:

http://hdl.handle.net/2433/281052

Analysis of End Effects in Diagonal Type MHD Generator by Means of Equivalent Circuit

By

Masaharu YOSHIDA* and Jūrō UMOTO*

(Received June 28, 1977)

Abstract

In this paper, there are analyzed current and potential distributions in the end region of a large scale combustion gas diagonal MHD generator by means of a new equivalent circuit. It is ascertained that the calculation results by the equivalent circuit method agree well with the results by the conventional finite difference method. It is made clear that in numerical analysis of the current and potential distributions, the nozzle or the diffuser, which is connected with the generator duct inlet or exit, respectively, must be taken at least to the extent of the duct hight.

Next, this paper discusses in detail the influences of the applied magnetic flux distribution, the load current, and the output electrode number etc. on the current concentration which occurs at the ends of the output electrodes.

1. Introduction

About an MHD generator, which can convert such primary energy as fossil fuel or atomic energy into electric power on a large scale and with high efficiency and low environment pollution, numerous experimental and theoretical studies are being carried out for its practical use, corresponding with the rapid increase of the electrical energy demand in recent years. Performance characteristics of the MHD generator have been investigated by the quasi one-, two-, or three-dimensional calculation method. The quasi one-dimensional theory[1] is very convenient for grasping the outline of the generator characteristics. However, by this theory, it is difficult to deal accurately with non-uniformity of a working gas plasma in the generator duct cross-section.

On the other hand, considering the imperfection of the quasi one-dimensional analysis, the two- or three-dimensional analysis was also developed by many workers. In their analyses[2,3], they have solved numerically the two- or three-dimensional partial differential equation for the current stream or potential function, which is derived

* Department of Electrical Engineering.

from Maxwell's equations, Ohm's law etc., or do directly and numerically the two- or three-dimensional MHD equations by the finite difference method.

Although the digital calculation by the difference analogue can give solutions with a high accuracy, the calculation needs very much computation time. Consequently, though it is suitable for a local analysis, it is unsuitable for the analysis of the whole generator.

On the other hand, as another two dimensional calculation for the Faraday or the Hall type MHD generator, an analysis using an equivalent circuit was proposed[4,5], by which we can calculate easily and closely the electrical quantities in the generator such as the current, the electrical power, the electrical efficiency etc.

Recently, the authors proposed a two-dimensional analysis of the diagonal type generator by means of a new equivalent circuit[6]. In this analysis, the effects of ion slip of plasma and finite segmentation of the electrode were newly considered in addition to the effects of the leakage current on the duct insulation wall and boundary layer, which have been considered in previous papers. Already, they have found out a fairly simple and suitable equivalent network for the central region of the generator duct[7], where the electrical properties can be assumed to vary periodically in the period of the electrode pitch along the gas flow. Further, for analyzing overall performance of the generator, it is necessary to discover not only the above suitable equivalent network for the central region but also proper ones for the inlet and exit areas of the generator.

Considering the above mentioned, this paper introduces a simple and suitable equivalent network for the inlet or exit region of a large scale combustion gas diagonal type generator. Comparing the numerical calculation examples of potential and current distributions in the generator duct by the new equivalent circuit method with those results by the conventional accurate finite difference method, it is ascertained that the equivalent circuit gives satisfactory calculation results. Further, there are investigated in detail influences of the applied magnetic flux distribution, the load current, the number of output electrode etc. on the current concentration at the ends of the output electrodes.

2. Equivalent Network of Diagonal Type Generator

2.1 Generator duct and distribution of applied magnetic flux

Figure 1 shows a schematic diagram of the region from the inlet or exit to the central part of the diagonal type MHD generator duct, which is adopted as the research object in this paper. In the figure, φ is the slant angle of the straight line joining the electrode pair to the gas flow direction, i. e. x-axis, N_{out} the number of the output electrodes which are shortend each other, N_{tran} the number of the

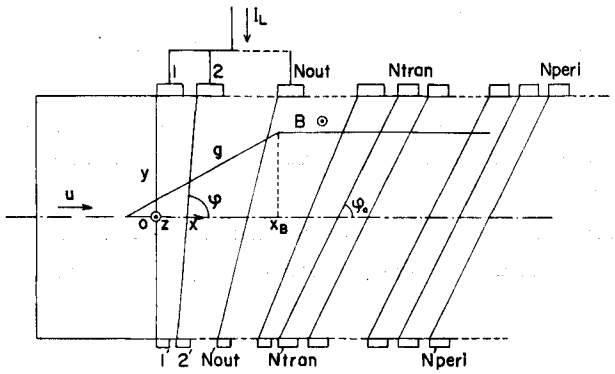

Fig. 1. Schematic diagram of end duct region of diagonal generator.

electrodes where $\varphi=\varphi_i$ reaches a constant angle φ_0 at the front location, according to the following relation

$$|\cot \varphi_{i+1}-\cot \varphi_i| = \cot \varphi_0/(N_{tran}-1), \qquad \cdots\cdots\cdots (1)$$

where $i=1, 2, \ldots, N_{tran}$, N_{peri} the number of the electrodes which the electrical properties can be assumed to be periodic after. N_{out} must be properly selected in accordance with the load current, and N_{tran} is decided almost by the value of φ_0. Besides, as N_{out}, N_{tran}, or x_B becomes large, or as φ_0 becomes small, N_{peri} must be taken large.

To investigate a influence of the attenuation of the applied magnetic flux density B on the current concentration at the output electrode ends, as shown in Fig. 1, it is assumed that B is constant in the central region, and decreases linearly from a point of $x=x_B$ at the rate of $g=dB/dx$ in the generator end regions. In addition, the secondary magnetic flux density induced by the generator current is assumed to be negligible compared with B, because the magnetic Reynolds number of the gas is much smaller than unity under the operating conditions. The electric conductivity σ and velocity u of the gas are assumed to be constant.

2.2 Space element and its equivalent circuit

In general, the physical properties of the working gas are not spatially uniform in the duct. Hence, let us divide the MHD generator duct space into many space elements, in which the electrical conductivity σ, the Hall parameter β, the current density $\boldsymbol{J}$, the electric field $\boldsymbol{E}$, the magnetic induction $\boldsymbol{B}$, the temperature T, the pressure p, the velocity $\boldsymbol{u}$ etc. all can be assumed constant. Then, we derive an equivalent circuit for the space element and eventually an equivalent network for the whole duct. In this connection, one of the space elements in the generator shown in

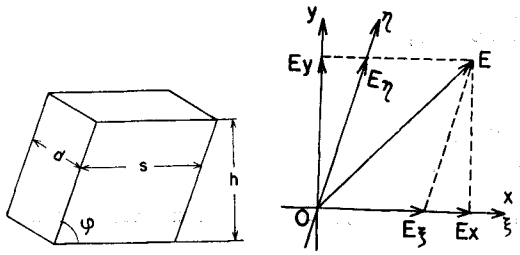

Fig. 2. Space element and coordinates.
(a) Space element.
(b) Coordinates.

Fig. 1 is given in Fig. 2(a), where s, h, d and φ are the length, height, width of the space element and the diagonal slant angle, respectively.

Now, as is well known, if the gradient of the partial electron pressure is negligible, a generalized Ohm's law[6] is given by

$$\boldsymbol{J}=\sigma\boldsymbol{E}'-\beta(\boldsymbol{J}\times\boldsymbol{B})/B+\beta\beta_i(\boldsymbol{J}\times\boldsymbol{B})/B^2, \qquad \cdots\cdots(2)$$

where

$$\boldsymbol{E}'=\boldsymbol{E}+\boldsymbol{u}\times\boldsymbol{B}, \qquad \cdots\cdots(3)$$

β and β_i are the Hall parameters for electron and ion, respectively, and E' is the electric field intensity vector in the coordinate system which moves with the gas velocity.

Next, let us assume $\boldsymbol{E}$, $\boldsymbol{J}$, $\boldsymbol{B}$ and $\boldsymbol{u}$ as follows;

$$\left.\begin{aligned}&\boldsymbol{E}=(E_x, E_y, 0),\ \boldsymbol{J}=(J_x, J_y, 0),\\ &\boldsymbol{B}=(0, 0, B),\quad \boldsymbol{u}=(u, 0, 0),\end{aligned}\right\} \qquad \cdots\cdots(4)$$

then, Eqs. (2) and (3) can be expressed two-dimensionally by

$$\begin{pmatrix}E'_x\\E'_y\end{pmatrix}=\begin{pmatrix}E_x\\E_y-uB\end{pmatrix}=\frac{1}{\sigma}\begin{pmatrix}1+\beta\beta_i & 1+\beta\beta_i\\ -\beta & \beta\end{pmatrix}\begin{pmatrix}J_x\\J_y\end{pmatrix}. \qquad \cdots\cdots(5)$$

Now, to simplify the analysis, let us introduce a new oblique coordinates (ξ, η) as shown in Fig. 2(b) for a space element $(d\times s\times h)$ given in Fig. 2(a). Then, the voltages V'_ξ and V'_η in the ξ and η directions, respectively, between both end surfaces of the space element are given by

$$\begin{pmatrix}V'_\xi\\V'_\eta\end{pmatrix}=-\begin{pmatrix}s & 0\\ h\cot\varphi & h\end{pmatrix}\begin{pmatrix}E'_x\\E'_y\end{pmatrix}. \qquad \cdots\cdots(6)$$

Also, the currents I_ξ and I_η in the ξ and η directions, respectively, in the space element are obtained as follows;

$$\begin{pmatrix} I_\xi \\ I_\eta \end{pmatrix} = \begin{pmatrix} dh & 0 \\ 0 & ds\sin\varphi \end{pmatrix} \begin{pmatrix} J_\xi \\ J_\eta \end{pmatrix}, \qquad \cdots\cdots(7)$$

where

$$\begin{pmatrix} J_\xi \\ J_\eta \end{pmatrix} = \begin{pmatrix} 1 & \cos\varphi \\ 0 & \sin\varphi \end{pmatrix}^{-1} \begin{pmatrix} J_x \\ J_y \end{pmatrix}. \qquad \cdots\cdots(8)$$

Using the Eqs. (5), (7) and (8), Eq. (6) is transformed as follows;

$$\begin{pmatrix} V'_\xi \\ V'_\eta \end{pmatrix} = \begin{pmatrix} V_\xi \\ V_\eta + e_\eta \end{pmatrix} = (Z) \begin{pmatrix} -I_\xi \\ -I_\eta \end{pmatrix}, \qquad \cdots\cdots(9)$$

where

$$\left.\begin{aligned} &\begin{pmatrix} V_\xi \\ V_\eta \end{pmatrix} = \begin{pmatrix} s & 0 \\ h\cot\varphi & h \end{pmatrix} \begin{pmatrix} E_x \\ E_y \end{pmatrix}, \\ &e_\eta = huB, \\ &(Z) = \begin{pmatrix} R_\xi & R_{mb} \\ -R_{ma} & R_\eta \end{pmatrix}, \end{aligned}\right\} \cdots\cdots(10)$$

in which

$$\left.\begin{aligned} &R_\xi = (1+\beta\beta_i)\,s/(\sigma dh), \\ &R_{ma} = \{\beta - (1+\beta\beta_i)\cot\varphi\}/(\sigma d), \\ &R_{mb} = \{\beta + (1+\beta\beta_i)\cot\varphi\}/(\sigma d), \\ &R_\eta = (1+\beta\beta_i)\,h/(\sigma ds\sin^2\varphi). \end{aligned}\right\}$$

From Eqs. (9) and (10), an equivalent four-terminal circuit for the space element in Fig. 2(a) is derived as shown in Fig. 3(a), where

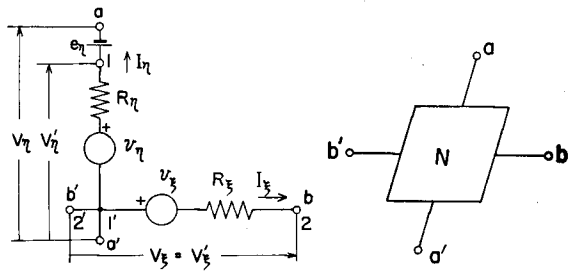

Fig. 3. Equivalent four-terminal circuit for space element
(a) Equivalent four-terminal circuit.
(b) Simplified illustration of (a).

$$v_\xi = R_{mb} I_\eta, \quad v_\eta = R_{ma} I_\xi. \qquad \cdots\cdots(11)$$

In addition, Fig. 3(b) is a simplified illustration of the equivalent circuit in (a).

2.3 Application of equivalent circuit to diagonal type generator

In an actual MHD generator, because of the spatial non-uniformity of the

physical quantities in the duct space, it may be thought that each space element has a considerably small volume as compared with the whole duct size. Accordingly, replacing each space element by the equivalent circuit in Fig. 3, the generator end region in Fig. 1 is denoted, for example, by an equivalent network as shown in Fig. 4.

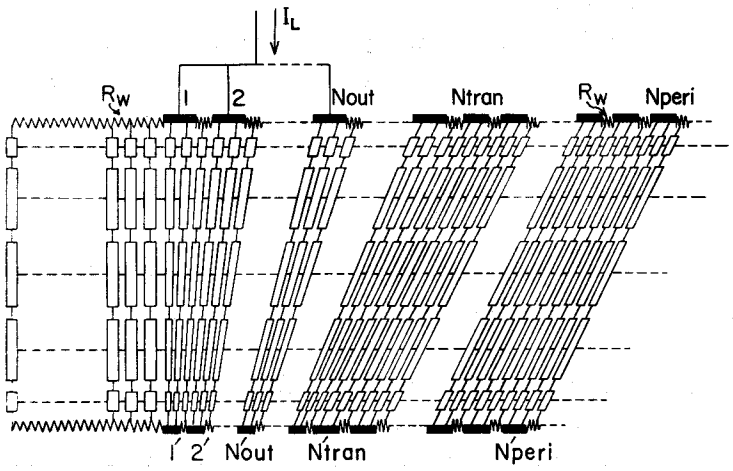

Fig. 4. Illustration of duct end region by equivalent networks.

As seen in the figure, the duct space between the anodes and cathodes is divided horizontally into five layers, where both the uppermost and the lowest layers are assumed much more thinner than the other three layers. The thicknesses of the former two layers are taken as being equal to each other, because it was ascertained that by such a treatment the accuracy of the numerical calculation by the equivalent circuit is well. Further, the domain of one electrode pitch along the gas flow is divided vertically into three columns: two with the electrode and one with the insulating spacer. Moreover, it is assumed that the sizes of the space elements in the nozzle region are comparable to the ones in the electrode region.

Also in Fig. 4, R_w is the equivalent leakage resistance along the insulator surface between the adjacent electrodes, and R_w' is the equivalent leakage resistance along the nozzle inner surface. In the numerical calculation, the values of R_w and R_w' are chosen as $10^4\Omega$, sufficiently large so as not to affect the calculation results. Later, it will be clarified that the above mentioned number and magnitude of the space elements present satisfactory numerical calculation results for the generator performance characteristics.

3. Calculation Methods

3.1 Analysis by equivalent circuit method (ECM)

As seen from Fig. 3(a) and Eqs. (10), the values of the resistances and electomotive forces in the equivalent circuit of each space element in Fig. 4 can be numerically determined when the dimension of each space element and σ, β and β_i in the element are given.

Next, many simultaneous circuit equations for the unknown currents flowing in the resistances in the equivalent network shown in Fig. 4 are obtained by Kirchhoff's law. When the simultaneous equations are numerically solved, the values of the currents and consequently their densities in the space elements are obtained Then, the potential of each electrode can be numerically calculated.

In this connection, the above simultaneous equations need much space to be recorded. Hence, for the purpose of page saving they are omitted in this paper, but one example can be seen in Ref. 7.

3.2 Analysis by finite difference method (FDM)

Up to now, usually the two-dimensional distributions of the current or the potential in the generator duct have been obtained by solving numerically the difference analogue of the partial differential equation for the stream function Ψ or the potential one Φ, which is derived from the Maxwell equations, a generalized Ohm's law, etc., under some appropriate boundary and subsidiary conditions.

The numerical calculation results by the FDM are highly accurate when the duct is divided into many fine meshes. Accordingly, by comparing the calculation results of the current and potential distributions in the duct ends by the ECM with the similar ones by the FDM under the same numerical conditions, the reliability of the ECM will be investigated.

Hitherto, by the FDM, only the differential equation for Ψ or Φ has been first solved numerically, and then the other quantities were obtained by using the value of Ψ or Φ. On the other hand, here it is tried to solve the equation for Φ in the duct region with electrodes and the equation for Ψ in the nozzle region without electrodes. Through practical calculation under the numerical conditions used in this paper, it was ascertained that the latter calculation method is superior to the former conventional one in the convergence speed.

In addition, the current and potential distributions in the exit region become symmetric to the one in the inlet region in the case where it can be assumed that the gradient of the partial electron pressure can be neglected as in our case.

4. Numerical Conditions

The conditions assumed for the numerical calculation are listed in Table 1, where they are the values almost corresponding to a practical MHD generator. In the table, H, S_e, C_e and I_L are the height, the one electrode pitch, the electrode width along the center line, and the load current, respectively. $N_{peri}=17$ and 32 are the numbers of the cathodes used in the analysis by the FDM, and more cathodes are used in the analysis by the ECM.

Table. 1. Numerical conditions used in calculation.

φ_0 (°)	45		68.2
Nout	1 to 10		6
Ntran	11		4
Nperi	32		17
$\mu=\beta/B$ (1/T)	1/6	2/3	1/6
I_L ($\times10^4$A)	6	0.1 to 3	4
x_B (m)	0, 1, 2, 3		—
g (T/m)	0, 1, 2.5, 5		0
H (m)	1.5		
S_e (m)	0.15		
C_e/S_e	0.65		
σ (℧/m)	10		
u (m/s)	800		
B_0 (T)	6		

5. Comparison of ECM and FDM

5.1 Comparison of ECM and FDM

Figures 5(a) and (b) show the potential and current distributions in the generator end region, respectively, which are calculated by the FDM with the conditions of $\varphi_0=45°$, $N_{out}=4$, $\mu=2/3$, $I_L=2\times10^4$A, $x_B=1.5$m and $g=2.5$T/m, where the contour intervals are 200V and 500A/m, respectively.

Figure 6 shows the distribution of the current density vectors in the space elements in the end domain which are obtained by the ECM under the same numerical conditions as in Fig. 5. In this figure, the maximum current density of 3.9×10^4A/m^2

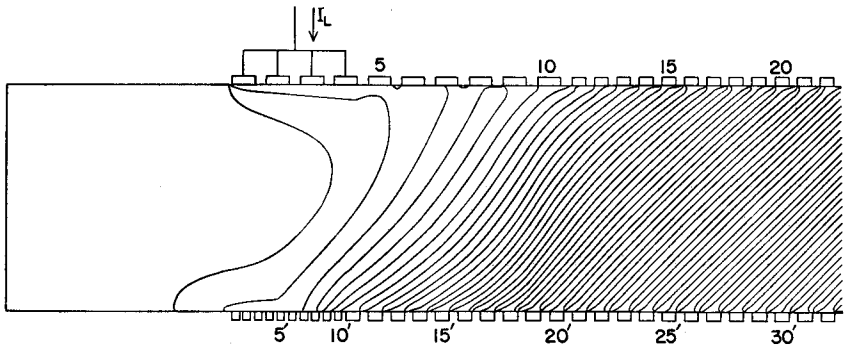

(a) Potential distribution (contour interval: 200V).

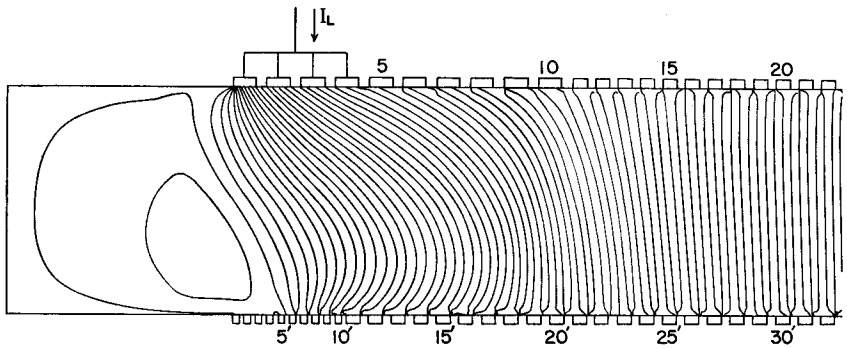

(b) Current distribution (contour interval: 500A/m).

Fig. 5. Potential and current distributions calculated by FDM ($\varphi_0=45°$, $N_{out}=4$, $\mu=2/3$, $I_L=2\times10^4$A, $x_B=2$m, $g=2.5$T/m).

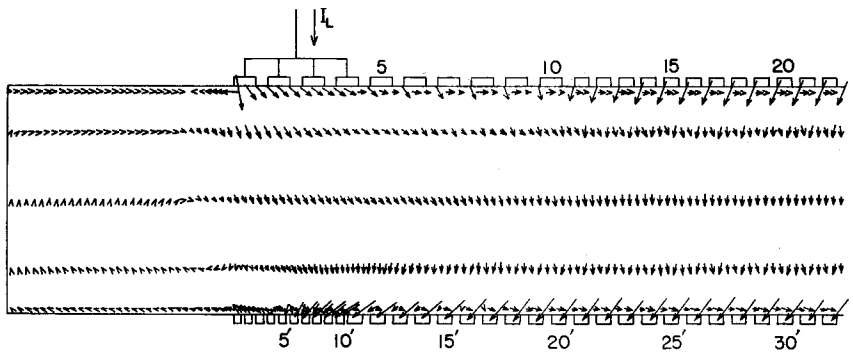

Fig. 6. Current pattern calculated by ECM for the same conditions as in Figs. 5. (maximum current density: 3.9×10^4A/m^2).

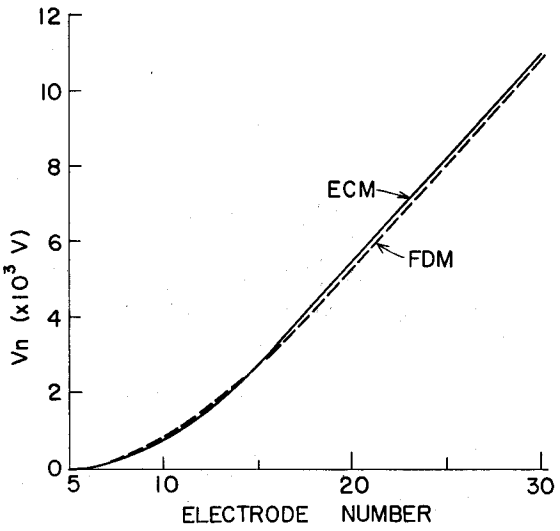

Fig. 7. Comparison of V_n calculated by ECM and FDM.

appears at the front end of the upper first output electrode 1. From Figs. 5(b) and 6, it will be seen that the current pattern in the latter is quite analogous to the one in the former.

Next, Figure 7 presents the potential differences V_n between the output electrodes and the n-th electrode ($N_{out} < n \leqq N_{peri}$), which are calculated by the FDM and the ECM. It is seen that the calculation result of V_n by the ECM sufficiently agrees with the one by the FDM.

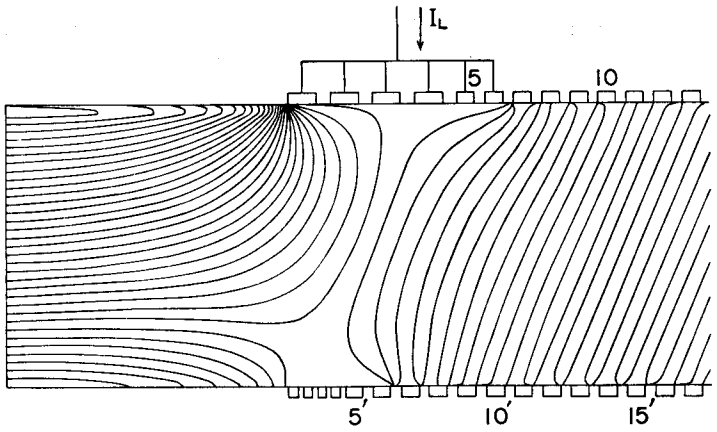

(a) Potential distribution (contour interval: 200V).

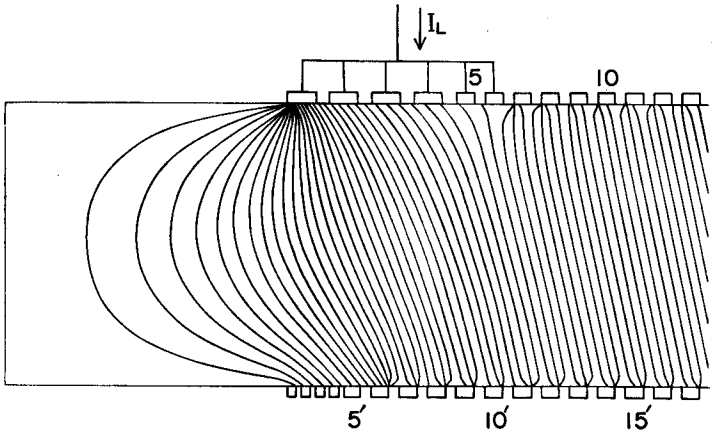

(b) Current distribution (contour interval: 1500 A/m).

Fig. 8. Potential and current distributions calculated by FDM ($\varphi_0=68.2°$, $N_{out}=6$, $\mu=1/6$, $I_L=4\times10^4$A, $g=0$).

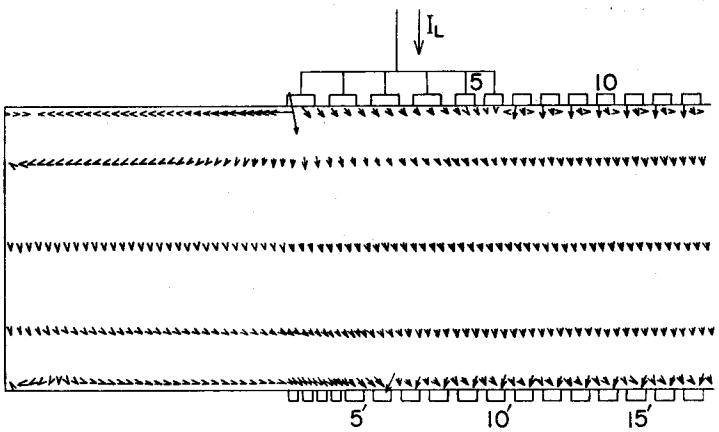

Fig. 9. Current pattern calculated by ECM for the same conditions as in Figs. 8. (maximum current density: 24.1×10^4A/m^2).

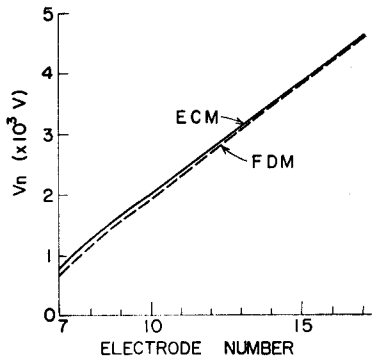

Fig. 10. Comparison of V_n calculated by ECM and FDM.

Next, in Figs. 8(a) and (b), there are plotted the potential and current distributions in the end area, respectively, which are obtained by the FDM for $\varphi_0=68.2°$, $\mu=1/6$, $I_L=4\times10^4$A and $g=0$, where the contour intervals are 200V and 1500A/m, respectively. On the other hand, Fig. 9 denotes the current pattern derived by the ECM under the same conditions as in Figs. 8. It will be recognized that the current pattern in Fig. 9 is sufficiently similar to the one in Fig. 8(b). In this connection, the maximum current density 24.5×10^4A/m^2 is found at the upstream end of electrode 1.

Next, in Fig. 10, there are plotted the potential differences V_n between the output electrodes and the n-th electrode, which are calculated by the above two methods. Again we see that the numerical results by both methods well accord with one another.

From the above explanation, it can be said that the calculation results by the ECM sufficiently agree with the highly accurate ones by the FDM and so are fully reliable.

In this connection, let us consider the following relations;

$$\left.\begin{aligned} E_y&=aE_x,\\ I_L&=A(J_x+aJ_y),\end{aligned}\right\} \qquad \cdots\cdots\cdots\cdots(12)$$

where $a=-cot\ \varphi_0$ is the inclination parameter and A the cross section of the duct. The above relations are the well known diagonal constraints used for the one-dimensional analysis. From Figs. 5(a) and (b), or 8(a) and (b), it will be seen that the relations (12) are no longer held due to distortions of the potential and current distributions in the end region with the output electrodes.

5.2 Electrical effect of nozzle or diffuser region near duct inlet or exit

The inlet and exit of an MHD generator duct are usually connected with a nozzle exit and a diffuser inlet, respectively. In the numerical calculation of the current and potential, the whole or a part of the above nozzle and diffuser regions must be also considered with the generator duct. Accordingly, in this article, let us discuss how long we should take the length L_{ins} of the nozzle or the diffuser in the flow direction which stand for the extent of the above regions.

Figure 11(a) shows the influence of L_{ins} on the current density J^*_{1u} at the upstream end of the upper first output electrode 1, and on $J^*_{1'u}$ at the same end of the lower first output electrode 1'. It also shows the potential difference V^*_5 between the output electrodes and electrode 5 which is nearest to them. Here, those values are normalized by the values of the similar current densities or voltage for $L_{ins}=2$m, respectively, and are obtained for $\varphi_0=45°$, $N_{out}=4$, $\mu=2/3$, $I_L=2\times10^4$A, $x_B=2$m

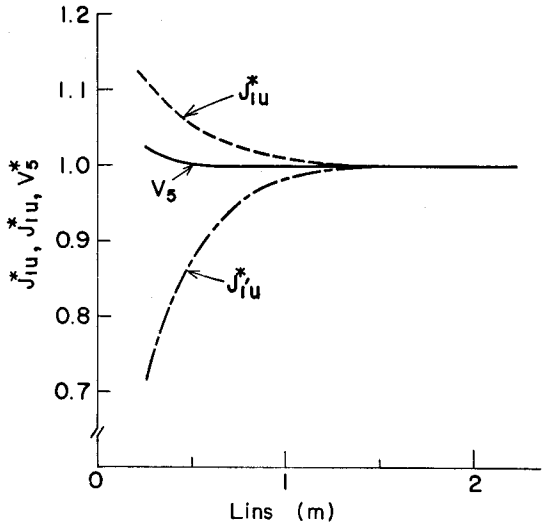

Fig. 11. Influence of *Lins* on J^*_{1u}, $J^*_{1'u}$, and V^*_5 ($\varphi_0=45$, $N_{out}=4$, $\mu=2/3$, $I_L=2\times10^4$A, $x_B=2$m, $g=2.5$T/m).

and $g=2.5$T/m by the ECM. From Fig. 11(a), it will be seen that we should take $L_{ins}\fallingdotseq 1.5$m, say $L_{ins}\fallingdotseq H$ for our duct size, to evaluate accurately the current concentration at the upstream ends of the output electrodes. On the other hand, we can satisfactorily calculate the potential of the electrodes with $L_{ins}=0.5$m, viz. $L_{ins}=H/3$. For the computation of the potential and current distributions already shown in Figs. 5(a), (b) and 6, $L_{ins}=1.5$m was used.

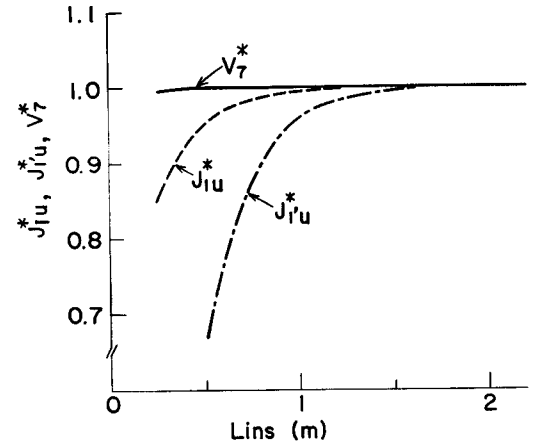

Fig. 12. Influence of L_{ins} on J^*_{1u}, $J^*_{1'u}$, and V^*_7 ($\varphi_0=68.2°$, $N_{out}=6$, $\mu=1/6$, $I_L=4\times10^4$A, $g=0$).

Next, Figure 12 denotes the influence of L_{ins} on J^*_{1u}, $J^*_{1'u}$, and V^*_7 which is the normalized voltage between the output electrodes and electrode 7, where $\varphi_0=68.2°$, $\mu=1/6$, $I_L=4\times10^4$A and $g=0$ are used. From this figure, it may be said that the conclusions in this case are almost the same as those obtained in Fig. 11, although a great deal of current flows into the nozzle region as seen in Fig. 8(b) and in Fig. 8(a), where we take $L_{ins}=1.5$m.

6. Current Concentration at Output Electrodes

6.1 Influence of distribution of applied magnetic flux

In Table 2(a), for the various values of x_B and g, there are shown the calculated results of the magnitudes J_{1u} and J_{4d} of the current density vectors $\boldsymbol{J}_{1u}$ and $\boldsymbol{J}_{4d}$ at

Table 2(a) Influence of x_B and g on current concentration ($\varphi_0=45°$, $N_{out}=4$, $\mu=2/3$, $I_L=2\times10^4$A).

x_B m	g T/m	$\bar{B}_{out}$ T	Upper Output Electrodes				Lower Output Electrodes			
			$\boldsymbol{J}_{1u}=(J_{1u},\theta_{1u})$ ($\times10^4$A/m^2, rad)		$\boldsymbol{J}_{4d}=(J_{4d},\theta_{4d})$ ($\times10^4$A/m^2, rad)		$\boldsymbol{J}_{1'u}=(J_{1'u},\theta_{1'u})$ ($\times10^4$A/m^2, rad)		$\boldsymbol{J}_{4'd}=(J_{4'd},\theta_{4'd})$ ($\times10^4$A/m^2, rad)	
—	0	6	20.2	−1.1	0.3	−1.3	0.3	2.9	7.4	−1.7
0	1	6	19.9	−1.1	0.3	−1.3	0.4	2.9	7.4	−1.7
	2.5	6	19.4	−1.1	0.3	−1.3	0.6	2.9	7.4	−1.7
	5	6	18.4	−1.1	0.3	−1.3	1.0	2.9	7.3	−1.7
1	1	5.30	18.1	−1.1	0.5	−0.8	0.6	2.9	6.5	−1.8
	2.5	4.24	13.7	−1.1	0.8	−0.5	1.3	2.7	4.7	−1.9
	5	2.48	4.5	−1.3	1.4	−0.4	2.2	2.2	1.0	−2.3
2	1	4.30	15.7	−1.1	0.7	−0.6	0.5	2.8	4.6	−1.8
	2.5	1.74	3.9	−1.4	1.5	−0.5	1.3	2.2	1.3	0.5
	5	0	0.6	−1.9	2.0	−1.0	1.2	1.6	4.8	0.2
3	1	3.30	12.5	−1.2	0.9	−0.5	0.4	2.7	2.5	−1.6
	2.5	0.02	0.6	−1.9	2.0	−0.9	1.1	1.6	4.7	0.2
	5	0	0.6	−1.9	1.7	−1.0	1.2	1.6	4.9	0.3

the front end of the upper first output electrode 1 and the rear end of the upper last output electrode 4, respectively, and the calculated results of the magnitudes $J_{1'u}$ and $J_{4'd}$ of the current density vectors $\boldsymbol{J}_{1'u}$ and $\boldsymbol{J}_{4'd}$ at the front end of the lower first output electrode 1 and at the rear end of the lower last output electrode 4', respectively, with the angles θ_{1u}, θ_{4d}, $\theta_{1'u}$ and $\theta_{4'd}$ which are the inclination angles of $\boldsymbol{J}_{1u}$ etc. to the x-axis. Also, in the same table, there are given the values of the average applied magnetic inductions $\bar{B}_{out}$ in the output electrode region

for the various x_B and g.

The table indicates that J_{4d} and $J_1'_u$ are small, in other words, the current concentration is not so intensive at the rear end of electrode 4 and the front end of electrode 1′. Also, it indicates that the smaller $\bar{B}_{out}$ becomes, J_{1u} becomes weaker. Accordingly, when x_B and g become large and therefore $\bar{B}_{out}$ becomes small, the current concentration is much more relaxed compared with the current concentration in the case of $g=0$. In this connection, the value of the current density at the electrode end in the periodic region becomes 3.1×10^4A/m^2. In the case of a large $\bar{B}_{out}$ J_{1u} is enormously large. For such phenomena, the following two reasons are considered. Firstly, as in the case of occurrence of the finite segmentation effect of the electrodes, the Hall electric field induced in the vicinity of the output electrodes is short-circuited by the electrodes of a finite width. Secondly, as seen from Fig. 8(a), even in the nozzle region near the output electrode 1, a large electromotive force is induced by the existence of the magnetic induction, and to compensate for the force, the current flows into the nozzle region from the upstream end of electrode 1.

Table 2(a) also shows that $J_4'_d$ is fairly heavy when $\bar{B}_{out}$ is large. This is also thought to be owing to the finite segmentation effect of the electrode. It is a noticeable tendency that as $\bar{B}_{out}$ decreases, $J_4'_d$ decreases first and then increases again. The reason why $J_4'_d$ becomes large in the case of $\bar{B}_{out}=0$ is perhaps that

Table 2(b) Influence of x_B and g on current concentration ($\varphi_0=45°$, $N_{out}=4$, $\mu=1/6$, $I_L=6\times10^4$A).

x_B m	g T/m	$\bar{B}_{out}$ T	Upper Output Electredes				Lower Output Electrodes			
			$J_{1u}=(J_{1u},\theta_{1u})$ ($\times10^4$A/m^2, rad)		$J_{4d}=(J_{4d},\theta_{4d})$ ($\times10^4$A/m^2, rad)		$J_1'_u=(J_1'_u,\ \theta_1'_u)$ ($\times10^4$A/m^2, rad)		$J_4'_d=(J_4'_d,\ \theta_4'_d)$ ($\times10^4$A/m^2, rad)	
—	0	6	24.2	−1.4	3.7	−0.7	1.7	−0.8	4.3	−0.3
0	1	6	23.5	−1.4	3.7	−0.7	1.4	−0.8	4.3	−0.3
	2.5	6	22.5	−1.4	3.7	−0.7	0.8	−0.8	4.3	−0.3
	5	6	20.7	−1.4	3.8	−0.7	0.1	2.4	4.3	−0.2
1	1	5.30	19.2	−1.4	4.2	−0.7	1.0	−0.9	5.3	0.1
	2.5	4.24	12.0	−1.5	4.8	−0.7	0.5	2.1	7.4	0.3
	5	2.48	3.5	−1.7	5.6	−0.7	2.5	1.8	10.6	0.4
2	1	4.30	14.8	−1.5	4.6	−0.7	5.9	−1.0	7.7	0.3
	2.5	1.74	3.5	−1.7	5.5	−0.8	2.4	1.7	12.7	0.4
	5	0	1.8	−1.9	5.1	−1.0	3.7	1.6	15.1	0.3
3	1	3.30	10.6	−1.6	5.0	−0.8	0.1	2.0	10.1	0.4
	2.5	0.02	1.8	−1.9	5.2	−0.9	3.7	1.6	15.0	0.3
	5	0	1.8	−1.9	5.0	−1.0	3.7	1.6	14.7	0.3

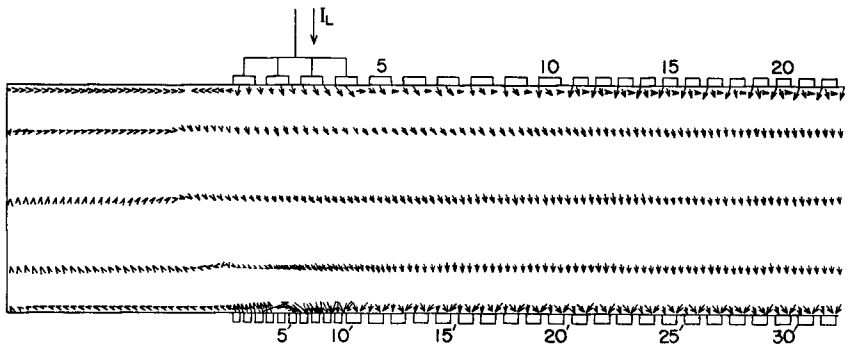

Fig. 13. Current pattern calculated by ECM ($\varphi_0=45°$, $N_{out}=6$, $\mu=1/6$, $I_L=6\times10^4$ A, $x_B=2$m, $g=2.5$T/m, maximum current density: 12.5×10^4A/m^2).

due to discrepancy of the electrode arrangements in the anode and the cathode, the electric field E_x near the lower down stream in the region with the output electrode is greater than the one near the upper down stream in the same region. Therefore, much load current flows out of the down stream end of electrode 4'.

Next, the digital calculation results similar to those in Table 2(a) are presented in Table 2(b), where $\varphi_0=45°$, $N_{out}=4$, $\mu=1/6$, and $I_L=6\times10^4$A. In general, the above concluding remarks obtained from Table 2(a) can be applied to the results in Table 2(b). Especially, in the case of $\bar{B}_{out}=0$, $J_4'_d$ increases very much. And comparing $J_4'_d$ in Table 2(a) with the same in (b), it may be said that $J_4'_d$ is almost proportional to I_L. For reference, Figure 13 shows the current pattern for the case where $\varphi_0=45°$, $N_{out}=4$, $\mu=1/6$, $I_L=6\times10^4$A, $x_B=2$m, and $g=2.5$T/m. The maximum current density of 12.7×10^4 A/m^2 appears at the down stream and of electrode 4'.

6.2 Influene of load current

Table 3(a) shows the calculated results of the current densities J_{1u}, J_{4d}, $J_1'_u$ and $J_4'_d$ with the angles θ_{1u}, θ_{4d}, $\theta_1'_u$ and $\theta_4'_d$ for the various load currents I_L in

Table 3(a) Influence of load current on current concentration ($\varphi_0=45°$, $N_{out}=4$, $\mu=2/3$, $x_B=2$m, $g=2.5$T/m, $\bar{B}_{out}=1.74$T).

I_L ($\times10^4$A)	κ_0	Upper Output Electrodes				Lower Output Electrodes			
		$J_{1u}=(J_{1u}, \theta_{1u})$ ($\times10^4$A/m^2, rad)		$J_{4d}=(J_{4d}, \theta_{4d})$ ($\times10^4$A/m^2, rad)		$J_1'_u=(J_1'_u, \theta_1'_u)$ ($\times10^4$A/m^2, rad)		$J_4'_d=(J_4'_d, \theta_4'_d)$ ($\times10^4$A/m^2, rad)	
0.1	0.97	2.9	−1.4	0.6	−1.1	0.5	−1.0	9.2	−2.2
1	0.69	3.4	−1.4	1.0	−0.6	0.4	2.2	4.3	−2.1
2	0.37	3.9	−1.4	1.5	−0.5	1.3	2.2	1.3	0.5
3	0.06	4.4	−1.4	2.1	−0.4	2.2	2.2	6.8	0.8

the case of $\varphi_0=45°$, $N_{out}=4$, $\mu=2/3$, $x_B=2$m and $g=2.5$T/m. In this table, the load current I_L is calculated by the following equation

$$I_L=A\sigma uB_0(\beta_0-a)(1-\kappa_0)/(1+\beta_0^2), \qquad \cdots\cdots\cdots(13)$$

where $a=-cot\ \varphi_0$ is the inclination parameter in the periodic region, β_0 the Hall parameter for B_0 and κ_0 (see Table 3(a)) is the load factor in the periodic region. From the table, it will be seen that J_{1u} increases more or less with the increase of I_L. On the other hand, $J_4'_d$ runs into electrode 4′ and decreases with I_L when I_L is small. When I_L is large, inversely it flows out of the same 4′ and increases with I_L. J_{4d} and $J_1'_v$ are always fairly smaller than J_{1u} and $J_4'_d$. The current patterns in the case of $I_L=2\times10^4$A are shown in Figs. 5(b) and 6. In addition, we get the interesting result that $J_1'_u$ and $\theta_1'_u$ vary with the increase of I_L. It suggests that the position of the eddy current change with I_L in the upstream region of the lower output electrode.

Table 3(b) Influence of load current on current concentraion ($\varphi_0=45°$, $N_{out}=4$, $\mu=2/3$, $x_B=1$m, $g=2.5$T/m, $\bar{B}_{out}=4.24$T).

I_L ($\times10^4$A)	k_0	Upper Output Electrodes				Lower Output Electrodes			
		$J_{1u}=(J_{1u}, \theta_{1u})$ ($\times10^4$A/m^2, rad)		$J_{4d}=(J_{4d}, \theta_{4d})$ ($\times10^4$A/m^2, rad)		$J_1'_u=(J_1'_u, \theta_1'_u)$ ($\times10^4$A/m^2, rad)		$J_4'_d=(J_4'_d, \theta_4'_d)$ ($\times10^4$A/m^2, rad)	
0.1	0.97	12.3	−1.1	1.2	−2.8	1.3	−0.4	25.4	−2.0
1	0.69	13.0	−1.1	0.5	−2.1	0.1	−0.4	15.6	−2.0
2	0.37	13.7	−1.1	0.8	−0.5	1.3	2.7	4.6	−1.9
3	0.06	14.4	−1.1	1.7	−0.2	2.6	2.7	6.4	1.0

Next, Table 3(b) shows the calculated values of κ_0, J_{1u} θ_{1u} etc. for the various values of the I_L's as in Table 3(a), in the case of $\varphi_0=45°$, $N_{out}=4$, $\mu=2/3$, $x_B=1$m and $g=2.5$ T/m. Although J_{1u} etc. in Table 3(b) are much larger than those in Table 3(a), the above conclusions derived from Table 3(a) can be nearly applied to Table 3(b).

6.3 Influence of number of output electrodes

In Table 4, there are listed the calculated values of J_{1u}, J_{Nd}, $J_1'_u$ and $J_{N'd}$ for the various values of N_{out} when $\varphi_0=45°$, $\mu=2/3$ and $I_L=2\times10^4$A, with θ_{1u}, θ_{Nd}, $\theta_1'_u$ and $\theta_{N'd}$, respectively, where J_{Nd} and $J_{N'd}$ are the magnitudes of the current density vectors $\boldsymbol{J}_{Nd}$ and $\boldsymbol{J}_{N'd}$ at the down stream ends of the output electrodes N_{out} and N'_{out}, respectively, and θ_{Nd} or $\theta_{N'd}$ the angle between the x-axis and $\boldsymbol{J}_{Nd}$ or $\boldsymbol{J}_{N'd}$, respectively. From Table 4, it is seen that J_{1u} decreases and reaches a constant value, and

Table 4 Influence of N_{out} on current concentration ($\varphi_0=45°$, $\mu=2/3$, $I_L=2\times10^4$A, $x_B=2$m, $g=2.5$T/m).

Nout	Upper Output Electrodes				Lower Output Electrodes			
	$J_{1u}=(J_{1u}, \theta_{1u})$ ($\times10^4$A/m^2, rad)		$J_{Nd}=(J_{Nd}, \theta_{Nd})$ ($\times10^4$A/m^2, rad)		$J_1'_u=(J_1'_u, \theta_1'_u)$ ($\times10^4$A/m^2, rad)		$J_{N'd}=(J_{N'd}, \theta_{N'd}$ ($\times10^4$A/m^2, rad)	
1	5.4	−1.3	3.6	−0.7	3.3	2.2	8.7	0.97
2	4.3	−1.4	2.4	−0.6	2.0	2.2	5.5	0.89
4	3.9	−1.4	1.5	−0.5	1.3	2.2	1.3	0.52
6	3.9	−1.4	1.1	−0.4	1.2	2.2	2.4	−2.1
8	3.9	−1.4	0.8	−0.4	1.3	2.2	5.3	−2.4
10	4.0	−1.4	0.4	−0.6	1.4	2.2	7.6	−2.5

J_{Nd} rapidly decreases as N_{out} increases. $J_{N'd}$ flows out of the electrode N'_{out} and decreases with N_{out} when N_{out} is small, and inversely, it runs into the electrode N'_{out} and increases with N_{out} when N_{out} is large, and $J_1'_u$ decreases first and then increases a little as N_{out} increases. In this connection, it is made clear that the electrical output power has the maximum value for $N_{out}=4$ to 6.

By the above discussion, to remove the current concentration and to make the generated power large, it is necessary to determine the suitable output electrode number N_{out}. The current pattern for $N_{out}=4$ was already shown in Figs. 5(b) or 6.

7. Conclusions

The main conclusions derived from the above numerical investigation are as follows:

(1) The current and potential distributions in the end region of a large scale combusion gas diagonal type MHD generator are analyzed by means of a new equivalent circuit. It is ascertained that the calculation results by the equivalent circuit method agree well with those by the conventional finite difference method.

(2) It is made clear that in the numerical analysis of the current and potential distributions, the nozzle or the diffuser, which is connected with the generator duct inlet or exit, respectively, must be taken at least to the extent of the duct height.

(3) In general, the current concentration occurs intensively at the upstream end of the upper first output electrode and at the downstream end of the lower last output electrode. The concentration can be removed by an appropriately applied magnetic flux distribution. As the number of output electrodes also gives influences on the current concentration, the generated power, etc., it must be suitably chosen.

The analysis of the MHD generator by the ECM will be continued for analyzing two- or further three-dimensionally and designing optimally the whole generator.

Acknowledgements

The authors wish to acknowledge the helpful suggestion and advice of Assistant Prof. K. Yoshikawa, Assistant M. Ishikawa, Institute of Atomic Energy, Kyoto University, and Mr. K. Komaya graduate student, Kyoto University.

References

1) K. Takano et al.; 13th Symp EAM, 1973.
2) M. Ishikawa et al.; THIS MEMOIRS, Vol. 39 part 4, 1976.
3) T. Hara et al.; Ann. Meat. Atom. Ener. Soc. Japan A37, 1977.
4) H. Shirakata et al.; J. Nucl. Sci. Technol. Vol. 10, No. 1, Jan. 1973.
5) Z. Celinski; Rozprawy Elektrotech. 17, 108, 1971.
6) M. Yoshida et al.; THIS MEMOIRS Vol. 36, part 4, 1875.
7) M. Yoshida et al.; Trans. IEE Japan Vol. 87-A, No. 3, Mar. 1977.
9) R. J. Rosa; "Magnetohydrodynamic Energy Conversion," p. 28 McGraw-Hill, 1969.